energy&fuels

Article

pubs.acs.org/EF

Biomass Pyrolytic Polygeneration of Tobacco Waste: Product Characteristics and Nitrogen Transformation

Hanping Chen, Guiying Lin, Yingquan Chen,* Wei Chen, and Haiping Yang

State Key Laboratory of Coal Combustion, Huazhong University of Science and Technology, 1037 Luoyu Road, Wuhan, Hubei 430074, People's Republic of China

Supporting Information

ABSTRACT: Conversion of waste to high-value products by pyrolysis is a suitable and harmless disposal technology for the abundant waste generated in the tobacco industry. To determine the optimum operational parameters for biomass pyrolytic polygeneration using tobacco waste as the feedstock, the product characteristics and nitrogen transformation were investigated from 250 to 950 °C. The highest low calorific values of gas and char were 13 MJ/m^3 at 750 °C and 15 MJ/kg at 450 °C, respectively. The optimum operating temperature recommended for biomass pyrolytic polygeneration of tobacco waste is 650 °C when the three products (char, oil, and gas) are balanced. The char formation process is divided into three stages: degradation (250−450 °C), reforming (450−650 °C), and condensation (>650 °C). Three types of N-containing structures are formed in chars: pyridinic N, pyrrolic/pyridine N, and quaternary N. Pyridinic N is dominant at low temperatures, whereas quaternary N becomes dominant at high temperatures. N-containing volatiles escape from chars with increasing temperature and are primarily found in oil below 550 °C and in gas above 650 °C. N-containing compounds are the major components (up to 45%) in the organic portion of oil, with pyridines, pyrroles, and piperidines as the dominant forms. In the gas product, NH_3 and HCN are the major N-containing compounds released above 650 °C. This study is expected to be beneficial for the comprehensive utilization of tobacco waste.

1. INTRODUCTION

Cigarette manufacturing is the pillar industry for some developing countries,[1,2] including China, the largest global producer.[3] However, disposal of the abundant tobacco waste is a major problem. Approximately 0.6−0.8 million tons of tobacco waste is generated in China annually,[3] but the majority of this waste is spread over the tobacco fields or landfilled by cigarette factories.[4] Harmful components, such as nicotine and other S-, P-, and N-based chemicals, leach into the soil and water causing serious environmental pollution when tobacco waste is spread over tobacco crops or landfilled.[2] However, tobacco waste has a high level of organic components and shows potential as a biomass resource for energy production. Therefore, it is necessary to determine an environmentally friendly and efficient conversion technology for utilization of tobacco waste.

Earlier studies of nicotine extraction[5] and conversion to other chemicals[6,7] have explored methods for nicotine collection. These reports provide conversion technologies for tobacco waste, in which the harmless, non-nicotine waste could be introduced into tobacco plants used as fertilizer or landfilled. Unfortunately, these technologies are too expensive for widespread use.

Over the past decade, conversion of tobacco waste to bioenergy or biofuel has attracted wide attention. Yang et al.[8] converted tobacco stems to heat and found that tobacco stem combustion worked well in fluidized beds and the combustion efficiency could reach 94%. Zhang et al.[9,10] studied the co-combustion characteristics between tobacco stems and coal. The result indicated that tobacco stems showed co-combusting performance similar to that of coal. However, the nicotine-enriched tobacco waste had a high N content;[2] therefore, massive NO_x emissions would be a critical issue to consider during the combustion of tobacco waste for bioenergy.

Pyrolysis can efficiently convert biomass to multiple products (char, oil, and gas), and utilization of such products could avoid the risks associated with the high N content of tobacco waste.[3,11−13] Cardoso et al.[11] found that the major component of the pyrolytic products from slow pyrolysis of tobacco waste was L-nicotine, which was present in much higher concentrations than in products derived from holocellulose or lignin. Strezov et al.[12] investigated the pyrolysis behavior and product characteristics of tobacco waste. The results indicated that the bio-oils contained complex chemical structures and the biochar exhibited enriched fixed carbon, ash, and nutrients P and K. In addition, nicotine was observed in the bio-oils, and N remained in the biochar at relatively constant concentrations throughout the pyrolysis process. Cardoso et al.[14] studied the influence of the temperature on the bio-oils from tobacco residue and found that the nicotine content decreased while other chemicals increased with increasing temperature. However, these studies were focused mainly on the bio-oils from tobacco waste, while biogas and biochar were not described in detail. Furthermore, no literature has reported the N transformation during pyrolysis. As such, it may not be beneficial to obtain an

Special Issue: 5th Sino-Australian Symposium on Advanced Coal and Biomass Utilisation Technologies

Received: September 29, 2015
Revised: November 25, 2015
Published: November 30, 2015

DOI: 10.1021/acs.energyfuels.5b02255
Energy Fuels 2016, 30, 1579−1588

optimum pyrolysis condition when N in tobacco waste could be used as N-containing chemical products.

In our previous study, biomass pyrolytic polygeneration technology was studied and the results demonstrated that this technology was a good method for biomass conversion;[15,16] hence, it has wide applications commercially.[17] The abundant resource of tobacco waste has attracted operators of biomass pyrolytic polygeneration to use tobacco waste as a feedstock for this system. In comparison to other biomasses, such as cotton stalk, rice husk, and bamboo, tobacco waste has higher ash and N contents, which may influence the properties of the products from biomass pyrolytic polygeneration. Conversion of N to suitable products is important when using tobacco waste as a feedstock in biomass pyrolytic polygeneration; hence, the N transformation and distribution in pyrolytic products should be investigated. However, there has been no literature focused on this point. In this study, the product characteristics and the basic information on N transformation, including distribution and form, in the three products were investigated over the 250−950 °C range to determine the optimum operating temperature for biomass pyrolytic polygeneration when using tobacco waste as feedstock.

2. MATERIALS AND METHODS

2.1. Materials. Tobacco waste was collected from Bijie, Guizhou Province in China, and naturally dried after being reaped. Samples were then stored in a room with good ventilation. Before the experiment, the samples were crushed and sieved to obtain a powder with a particle size of <1 mm and an average particle size of ∼353 μm.

The tobacco waste consisted of 34.14% C, 4.37% H, 29.08% O, 2.42% N, and 0.44% S on a dry weight basis, which was measured using a Vario EL II elemental (CNHS/O) analyzer (Germany). The N content is rather high compared to other biomasses. Proximate analysis performed on an air-dried sample indicated 63.56% volatile matter, 5.23% moisture, and 24.33% ash, resulting in a rather low fixed carbon content (6.89%), which was measured using a SDTGA-2000 analyzer (Navas Instruments, Spain). The high ash content presents a problem because it limits the thermal conversion.[8] Furthermore, the acid extraction (pectin), hemicellulose, cellulose, and lignin contents of the dry sample were 15.21, 11.78, 26.43, and 18.63%, which were measured using the Van Soest method. The lower heat value of the air-dried sample of tobacco waste was 12.34 MJ/kg, measured using an oxygen bomb calorimeter (Parr 6300, Moline, IL).

2.2. Pyrolysis Experiment. The pyrolysis of tobacco waste was carried out in a fixed-bed reactor shown in previous works.[15,16] In brief, this pyrolysis system composed of a vertical tube (inner diameter of 38 mm and height of 600 mm), an electrical furnace, a gas-condensing system, and an incondensable gas collection and analysis system. The tube was preheated to the selected temperature (250, 350, ..., 950 °C) previously. After the temperature stabilized, about 3 g of tobacco particle was placed in the center of the reactor quickly and kept for 30 min. The samples were heated rapidly and decomposed promptly, and the volatiles were purged out with pure N_2 stream (99.99%, 1 L/min). The condensable volatiles were condensed and collected in an ice−water condenser as liquid product, whereas the non-condensed parts were cleaned through a glass wool filter, dried using silica gel, and finally collected using a gasbag as the gas product. After each trial, the reactor was brought back from the furnace to the ambient environment and rapidly cooled using a cooling fan. The residue of pyrolysis was weighed and recorded as the solid charcoal yield. The yields of gas and liquid products were referenced to previous works.[15] The gaseous yield was calculated by combining the volumes of all of the gases collected during pyrolysis, with the volume then being converted to weight percentage at ambient temperature and atmospheric pressure (the volume of 1 mol of gas equals 24.45 L at 1 atm and 25 °C). The liquid product consisted of bio-oil, water, and some fine particles, and its yield was obtained by calculating the increase in weight of the condenser system. Each test was carried out at least 3 times, and all of the data provided for the product yield were the average value of three trials. As shown in Figure 1, the repeatability

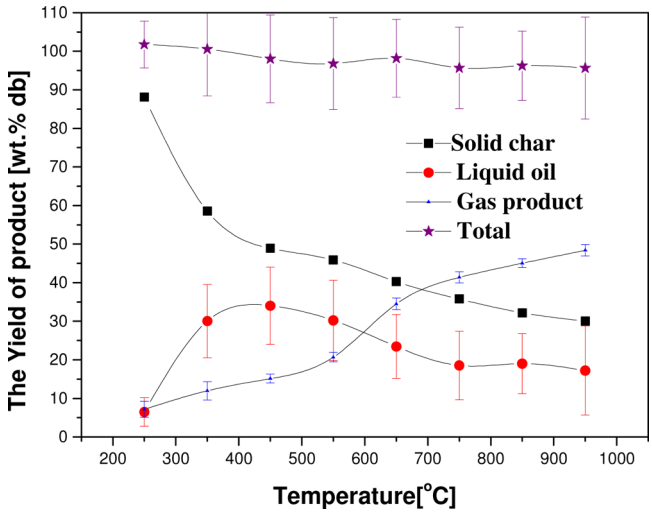

Figure 1. Yield distribution of tobacco waste pyrolysis at different temperatures.

of the char yield was the best, whose error was below 1%, while the repeatability of gas and liquid yields was relative worse, whose errors were 3−30 and 30−67%, respectively. The high error value of the liquid yield might be major, caused by the large weight difference between the condenser system and the increment of oil, above 300 g versus below 1.5 g, which could cause a large weight error.

2.3. Analysis of the Product. *2.3.1. Analysis of Gas and Oil Products.* A dual-channel micro-GC system (Micro-GC 3000A, Agilent Technologies, Santa Clara, CA), equipped with thermal conductivity detectors, was used to analyze qualitatively and quantitatively the gas product. The water content of liquid oil was measured by Karl−Fischer titration (TitroLine KF-10, Schott, Germany) according to the ASTM D1744 protocol prescribed by ASTM International (titrant, hydranal composite 2, Metrohm 787 KFTitrino). The main components of the bio-oil were determined in detail using gas chromatography−mass spectroscopy (GC−MS, HP7890 series GC with a HP5975 MS detector). The ultimate analyses of produced oil for carbon, hydrogen, and nitrogen were carried out with a CHNS/O elementary analyzer (Vario Micro cube, Germany). The pH of liquid oil was measured using a digital pH meter (S21 compact pH testers, Mettler Toledo). The concentration of NH_3 and HCN was off-line measured by a Fourier transform infrared spectroscopy (FTIR) analyzer (Gasmet DX4000).

2.3.2. Analysis and Characterization of the Char Product. Proximate analyses of solid charcoals were conducted using ASTM standards to obtain the moisture content, volatiles, fixed carbon, and ash content. Ultimate analyses of the dried samples for carbon, hydrogen, nitrogen, and sulfur were carried out with a CHNS/O elementary analyzer (Vario Micro cube, Germany). The calorimetric values of the dried samples were measured by bomb calorimetry (Parr 6300, Moline, IL). The particle size distribution and helium density of the char product were measured using a British particle size analyzer (Master Min, Malvern 2000, U.K.) and a commercial helium pycnometer (model 1330, Micromeritics Instrument Corporation), respectively.

The porosity property of solid char was measured with N_2 adsorption at a liquid nitrogen temperature (77 K) using a Micromeritics micropore analyzer (ASAP 2020, Norcross, GA). Before the adsorption measurements, the sample was degassed at 150 °C under a vacuum (pressure of 50 μm Hg) for 10 h. The pore size distribution was analyzed by the density function theory (DFT) method, which can be used to calculate the distribution of micropores

DOI: 10.1021/acs.energyfuels.5b02255
Energy Fuels 2016, 30, 1579−1588

(<2 nm), mesopores (2−50 nm), and macropores (>50 nm) simultaneously.

The organic function groups of solid biochar were analyzed with FTIR (VERTEX 70 spectrometer, Bruker, Germany) with a wavenumber between 4000 and 400 cm^{-1}. To deeply understand the evolution of chemical function groups in variant chars, generalized two-dimensional perturbation correlation infrared spectroscopy (2D-PCIS) was used. Its detailed introduction and treat procedure can be referenced to our previous work.[18] In brief,[18] 2D-PCIS can generate synchronous and asynchronous two-dimensional (2D) correlation intensity, which both represent as schematic contour maps, where two types of peaks are represented as two different correlations. One is autopeak (on the $w_1 = w_2$ diagonal), which is unique to the synchronous 2D correlation associated with positive correlation values and represents the vibrations most susceptible to changes in the external temperature T. The other is cross-peak (in off-diagonal positions, $w_1 \neq w_2$) in the synchronous and asynchronous 2D spectrum associated with a positive or negative correlation value and represent the general direction and sequence of change in w_1 compared to w_2 with T, respectively. The relative concentration (I_v/I_{max}) for different functional groups in the chars was defined, where I_v was the infrared (IR) intensity using Kubelka−Munk units at the characteristic wavenumber for a given functional group and I_{max} was the maximum intensity for the given functional groups across the chars.

The Fourier transform−Raman (FT−Raman) spectra of the samples between 1800 and 800 cm^{-1} were also recorded by this spectrometer. The detailed analysis procedure can be found in previous work.[15] The Raman spectra in the range between 800 and 1800 cm^{-1} were curve-fitted by the Opus software (version 6.00) with 10 Gaussian bands, as recommended by Li and co-workers.[19] The 10 Gaussian bands shown in Table 1S of the Supporting Information represent some typical structures.

The nitrogen-containing functional groups on the surface of biochar were analyzed with X-ray photoelectron spectroscopy (XPS, AXIS Ultra DLD, Kratos, U.K.) with Al Kα line (15 kV, 10 mA, and 150 W) as a radiation source. The C 1s peak position, set at 250 eV, was used as an internal standard. The curves on N 1s XPS peaks were fitted by XPSPEAK 4.1 software.

The measurement of water adsorption capacity was obtained using a controlled humidity chamber (HWS-150, Sengxin Corp., China) with a relative humidity (RH) of 90% at 30 °C. The solid samples (~2 g) were dried in a convection oven at 105 °C for 30 h and then immediately transferred to these chambers, where the samples resided about 3−12 days to reach equilibrium. The adsorption of phenol was measured according to the GB/T 12496.12-1999 protocol. About 200 mg of char samples and 50 mL of phenol solution (C_0 = 1 g/L) were put into an Erlenmeyer flasks (250 mL). The Erlenmeyer flasks were agitated in an orbital shaker for 2 h at room temperature and then left to rest for 22 h until filtered. The residual phenol concentration was analyzed at 269.5 nm using a Lambda 35 ultraviolet (UV) spectrophotometer (PerkinElmer, Waltham, MA). The adsorption capacity of phenol was calculated from the difference of initial and residue phenol solution concentrations.

3. RESULTS AND DISCUSSION

3.1. Product Distribution and Properties of Gas/Liquid Products. The char, oil, and gas yields at various temperatures are shown in Figure 1. At 250 °C, the degradation of tobacco waste is insignificant; hence, the char yield is 88 wt %. However, when the temperature is increased to 350 °C, the char yield decreases to 58 wt %. Subsequently, a decrease in the char yield, from 58 to 30 wt %, is observed from 350 to 950 °C. This suggests that major degradation reactions occur at 250−350 °C. The volatiles extracted from the solid residue during pyrolysis are present in the oil and gas products. With the temperature increase, the distribution of these volatiles in oil and gas changes. Below 600 °C, volatiles are primarily found in the oil, with the maximum yield of ~34 wt % at 450 °C. At temperatures over 600 °C, more gas product is formed and the maximum yield is 48 wt % at 950 °C.

The accumulated amount of gas released at the various pyrolysis temperatures is shown in Figure 2. The main gas

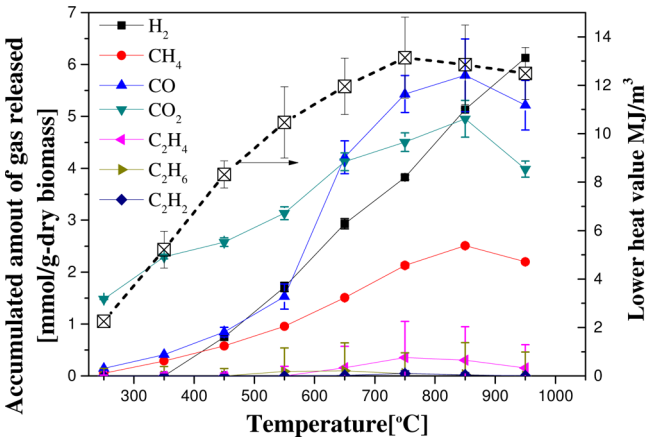

Figure 2. Accumulated amount of gas released at different pyrolysis temperatures.

products are H_2, CO_2, CO, and alkanes (CH_4, C_2H_4, C_2H_6, etc.), which is consistent with previous reports.[12,15] CO_2 is observed first and is dominant at 250 °C. The CO_2 concentration continues to increase to a maximum of ~4.95 mmol/g of dry biomass until the temperature reaches 850 °C. Generally, CO_2 is formed by decarboxylation of hemicellulose and cellulose at low temperatures and is no longer released above 550 °C.[15] However, the continued release of CO_2 from 550 to 850 °C for tobacco waste is slightly different from cotton stalk,[15] which may be influenced by further decarboxylation of volatiles during the secondary reaction. Below 550 °C, CO releases slowly, only 1.53 mmol/g of dry biomass at 550 °C; however, a sharp increase of CO is observed from 550 to 750 °C, up to 5.43 mmol/g of dry biomass, and the released amount is almost constant at high temperatures (>750 °C). This is consistent with other research,[12] in that released CO peaks in the temperature range of 550−750 °C; however, unlike the previous study, the amount of released CO is greater than that of CO_2 at this temperature. This may be due to the much longer residence time in the reactor. Moreover, the secondary reaction of volatiles and the decarbonylation in solid residue occur together; hence, more CO is released. No H_2 is released below 350 °C; however, a rapid and linear increase of H_2 is observed as the temperature increases from 350 to 950 °C, with a maximum yield of 6.12 mmol/g of dry biomass. In comparison to cotton stalk,[15] the initial releasing temperature is a bit lower, shifted from 450 to 350 °C, and the amount of H_2 is higher. This might occur because tobacco waste has a higher acid extraction content (15.21 wt %), in which the major component is protein.[3,12] Protein is easy to crack at lower temperatures and leads to some H_2 evolution.[20] CH_4 shows a similar trend to H_2, and the release of CH_4 is also affected by the high content of protein.[20] The continued increase of CH_4 is observed until a temperature of 850 °C, which may be due to demethoxylation of lignin in the solid residue or the release of volatiles during the secondary reaction.[12,15] With respect to the C_2 species, C_2H_4 shows a conspicuous release from 650 to 950 °C compared to the other two C_2 gas species. The low calorific

DOI: 10.1021/acs.energyfuels.5b02255
Energy Fuels 2016, 30, 1579−1588

value of gas obtained at 250 and 350 °C is <7 MJ/Nm^3, which is the lowest requirement for gas fuel supplied to urban residents (GB 50028-2006, China National Standard). Hence, the gas product obtained at 250 and 350 °C cannot be sold as gas fuel. With the increase in combustible composition, the low calorific value also increases from 8 to 13 MJ/m^3 as the temperature increases from 450 to 750 °C. Similar to cotton stalk,[15] at temperatures of >750 °C, the low calorific value remains at 12−13 MJ/m^3; hence, the optimum operation temperature for biogas is 750 °C.

Figure 3 shows the accumulated composition of liquid oil at various pyrolysis temperatures by GC−MS. The main liquid species are acids, furans, alcohols, cyclopentenes, ketones, phenols, fusing rings, and N compounds. In the investigated temperature range, four groups, acids, furans, cyclopentenes, and ketones, decrease with the temperature increase. The furan and cyclopentene contents are 20 and 10% at 250 °C, respectively, because they are mainly derived from hemicellulose and cellulose degradation,[21,22] and when the temperature is >650 °C, they diminish quickly. At low temperatures (<350 °C), ketones and acids are the main components; however, they diminish quickly with increasing temperature (350−850 °C). Consequently, other components are released, replacing ketones and acids, as the sample undergoes greater decomposition at higher temperatures. Phenol is mainly released at 250−350 °C, and subsequently, the content gradually increases to 25% at 850 °C. Phenols generally form below 650 °C, during the major degradation period of lignin;[21] however, the presence of phenols above 650 °C in the current study may be due to further decomposition of char or volatiles.[22] Fused rings are almost undetectable until 550 °C; however, a conspicuous release occurs after 650 °C, and the maximum value at 950 °C is close to 30%. These fused rings may be mainly formed during the condensation and structure reforming of char.[22] Alcohols display a trend in which they initially increase to achieve the maximum value (8%) and then quickly decrease with further temperature increases. Furthermore, alcohols disappear above 650 °C, which may be due to their low stability at high temperatures. N compounds show trends similar to alcohols; however, the maximum value (43%) is achieved at 550 °C. Furthermore, a sharpened decrease is observed at temperatures higher than 750 °C, which may be due to the secondary decomposition of these compounds at high temperatures. The detailed composition of N compounds will be discussed in section 3.3 to analyze the N transformation during pyrolysis.

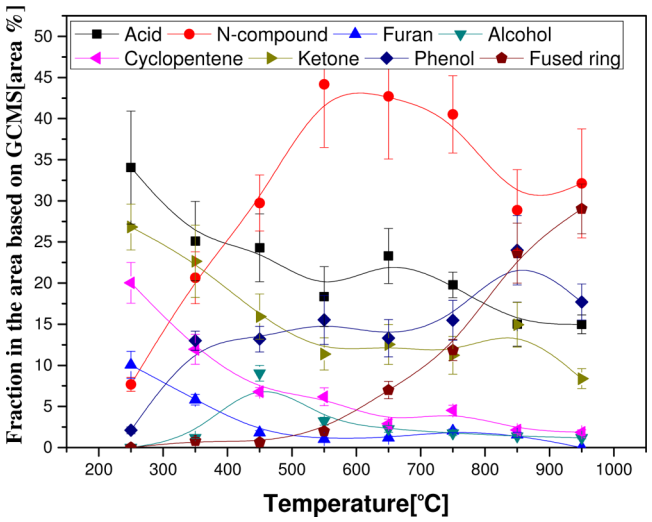

Figure 3. Accumulated amount of grouping composition in liquid oil at varied pyrolysis temperatures by GC−MS.

To determine the optimum operating temperature based on the liquid oil properties, the amounts of water, acetic acid, and phenol in liquid oil as well as the pH were analyzed quantitatively, and the results are shown in Table 1. The ultimate analysis shows that the carbon content is 15−29 wt %, which means that the organic component of oil is rather low as a result of the high water content of 53−60 wt %. With the temperature increase, the carbon content initially increases, reaches a maximum (28.57%), and subsequently begins to decrease. The H_2 content trend is similar to that of carbon; however, its peak temperature is 450 °C instead of 550 °C. It is notable that the N content of oil is higher than that of other biomasses.[20,23,24] The high N content of oil may be due to the high N content of tobacco wastes. The N content also reaches a maximum value at 550 °C but shows a slight decrease at higher temperatures. The acetic acid and phenol contents are also obtained. Acetic acid continues to decrease, whereas phenol shows an increasing trend. Although acetic acid is as high as 11.17 wt %, the high N content dictates that the oil cannot be used to refine acetic acid. The pH further indicates the effect of a high N content. With the increase in N, the pH increases because these N compounds create a basic environment.[20]

The utilization of oil from tobacco stems might be implausible, because the high N content leads to large amounts of NO_x when the oil is used as a liquid fuel. However, the N compounds can be refined and converted to N-containing chemicals, which is a promising way for tobacco waste utilization. In summary, 550 °C is the optimum operating temperature for high N-containing liquid oil derived from tobacco waste pyrolysis, because the oil yield and content of N-containing compounds are maximized.

Table 1. Evolution of the Amount of Water, Acetic Acid, and Phenol and the pH in Liquid Oil from Different Temperatures

temperature (°C)		250	350	450	550[a]	650	750	850[a]	950
ultimate analysis[b] (wt % of oil)	C	15.62	22.44	28.32	28.57	23.62	24.23	19.22	19.12
	H	3.43	4.27	4.97	4.77	4.24	4.14	3.27	2.76
	N	2.11	2.7	3.14	3.95	3.26	3.37	3.41	3.46
compostion (wt % of oil)	water	60.47	58.23	58.64	56.25	55.74	53.47	56.14	56.84
	acetic acid	11.17	8.60	7.44	5.86	7.43	6.35	4.08	4.39
	phenol	0.24	0.40	0.43	0.59	1.64	2.29	3.12	1.53
pH		3.1	4.1	4.2	5.8	5.6	5.7	5.7	4.9

[a]The data were repeated, and the errors were below 20%. [b]The analysis was on the basis of received oil.

DOI: 10.1021/acs.energyfuels.5b02255
Energy Fuels 2016, 30, 1579−1588

Table 2. Analysis of Chars at Different Temperatures

temperature (°C)	250	350	450	550[a]	650	750	850[a]	950
			Ultimate Analysis (on a Dry and Ash-Free Basis, wt %)					
C	53.54	60.18	61.59	63.79	66.15	66.88	76.38	88.15
H	5.11	4.03	3.06	1.35	2.29	1.34	1.29	1.08
N	4.05	4.25	4.13	4.14	3.88	4.3	3.72	1.45
S	0.75	0.79	0.91	0.7	0.86	0.8	0.92	1.54
O	36.55	30.75	30.31	30.02	26.82	26.68	17.69	7.78
			Proximate Analysis (on Dry Basis, wt %)					
volatile	67.06	62.46	53.50	44.58	39.38	34.37	29.82	23.74
ash	25.67	30.20	33.12	36.87	40.92	43.56	45.83	49.80
fixed carbon	7.27	7.34	13.38	18.55	19.7	22.07	24.35	26.46
LHV (MJ/kg)	13.77	14.27	15.03	14.67	14.12	14.89	13.96	11.23
			Physical Property					
particle size $D[4,3]$[b] (μm)	339	329	312	295	293	286	284	280
true density[a] (g/cm^3)	1.62	1.62	1.77	2.00	2.06	2.20	2.22	2.20

[a]The data were repeated, and the errors were below 10%. [b]$D[4,3]$ is the equivalent spherical diameter calculated from the particle size distribution.

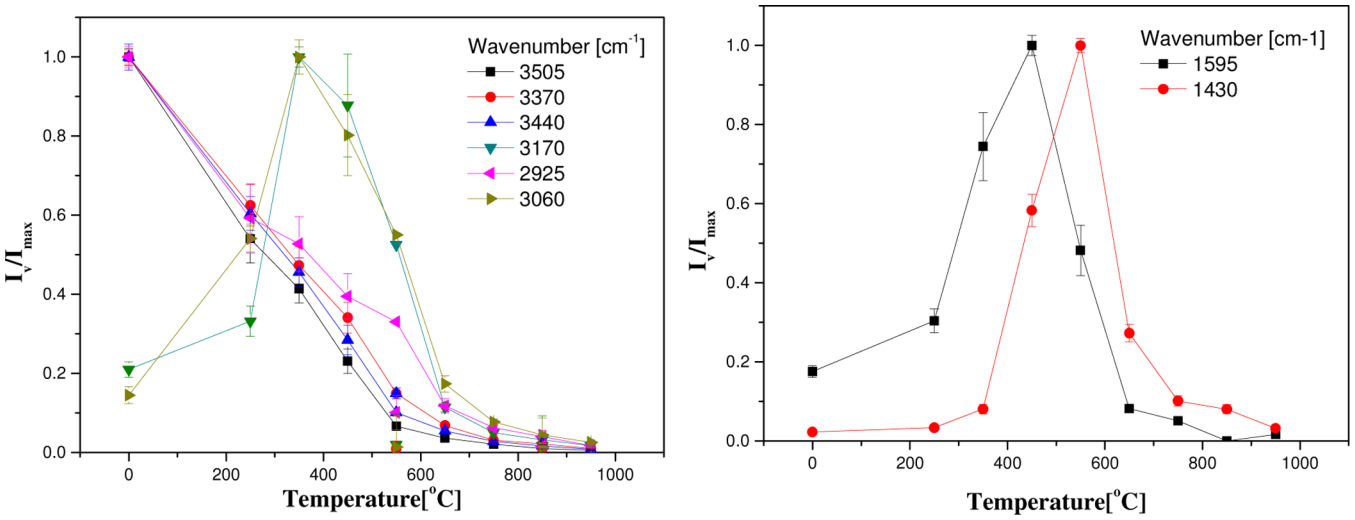

Figure 4. Variation in relative intensities (I_v/I_{max}, for peaks in synchronous 2D-PCIS spectra) for chars.

3.2. Characteristics and Structure Evolution of the Char Product. Table 2 lists the basic properties of chars. In the proximate analysis, the volatile content decreases with the temperature increase, while ash and fixed carbon increase. The result of the ultimate analysis shows that the carbon content in solid char first increases from 53.54 to 60.18 wt % with the temperature increase from 250 to 350 °C, while the H and O contents decrease greatly as a large amount of volatiles evolve. The carbon content then gradually increases to 66% at 750 °C; however, the H content decreases greatly, while the O content shows no obvious diminishment. This might indicate the cracking of mainly H-containing compounds. The 75% carbon content increases considerably to 88.15% with a further increase in the temperature (>750 °C). However, unlike at low temperatures (<750 °C), O shows an obvious decrease at the temperature above 750 °C, which might be due to the secondary cracking of O-containing components (C−O, C═O, etc.).

Unlike chars from other biomasses,[15,25−28] the N content of tobacco waste char is high, up to 3−4 wt %, while the N content of chars from other woody or agriculture biomasses are <1 wt %. This will limit the char from tobacco waste as a solid fuel because of the notable potential NO_x pollution; however, it may be used as biochar because N is an important nutrient for soil and plants.[29]

In addition, the calorific values of the chars show a slight increase to a maximum of 15 MJ/kg at 450 °C and then remain at 13−14 MJ/kg until 850 °C. The average particle size and density are also obtained. In comparison to the raw sample, chars experience a significant volume shrinkage and the degree of shrinkage increases with the temperature until 750 °C, while the particle volume shrinkage ceases above 750 °C. The volume shrinkage may be due to the removal of volatiles and the structure transformation during carbonization. With the increased release of low-density volatiles and ash from chars, the density of chars dramatically increases from 1.62 to 2.22 g/cm^3 until 750 °C and then remains at 2.2 g/cm^3 as the temperature continues to increase.

Figure 1S of the Supporting Information shows 2D-PCIS spectra of chars at various temperatures. The auto-peaks in the synchronous 2D spectra indicate that three functional groups are most susceptible to changes effected by the temperature: the H bond in R−NH_2 at 3370 cm^{-1}, the C−H bond in methyl or methylene at 2925 cm^{-1}, and the O−C−N−H stretch in R−CO−NH_2 at 1430 cm^{-1}.[15,30,31] As shown in Figure 4, the intensities of the H bond in R−NH_2 and the C−H bond in methyl or methylene significantly decrease when the temper-

DOI: 10.1021/acs.energyfuels.5b02255
Energy Fuels 2016, 30, 1579−1588

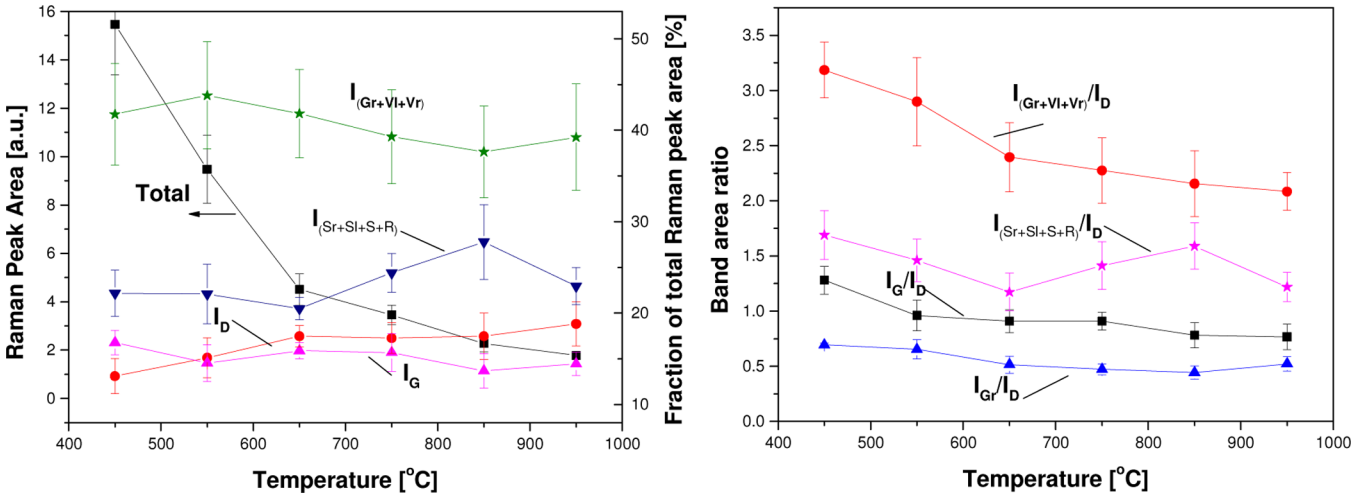

Figure 5. Raman peak areas and band ratios as functions of the pyrolysis temperature for the chars.

ature increases from 250 to 650 °C and both groups disappear above 650 °C. This may reveal that the decomposition of protein and lignin, represented by the H bond in R−NH_2 and the C−H bond in methyl or methylene, mainly occurs at a temperature of <650 °C. The intensity of the O−C−N−H stretch in R−CO−NH_2 initially increases to a maximum at 550 °C and decreases as the temperature increases. Below 350 °C, this group is not observed; however, it forms dramatically at 350−550 °C and is immediately removed at 550−750 °C. R−CO−NH_2 may be formed in the cross-linking reaction between protein and holocellulose or lignin.[20,32] The cross-peaks in the synchronous 2D spectra show that the vibration at 3060 cm^{-1} has an opposite direction to that of the vibration at 3370 cm^{-1}. The vibration at 3060 cm^{-1} represents the NH bond in the NH_3^+ group.[30] NH_3^+ is formed when −NH_2 adsorbs a proton (H^+), which may be from the cleavage of OH or CH in holocellulose or lignin. The evolution of I_v/I_{max} shows that this group mainly forms at 250−350 °C and is removed at 350−650 °C. During the formation process, N-compounds are rare, while large amounts of N compounds are released during the removal process. This suggests that the proteins in tobacco waste may behave as proton acceptors during the early decomposition reaction. Furthermore, the results of the asynchronous 2D spectra show that the vibrations at 3505 and 3440 cm^{-1} change before 3370 cm^{-1}, which represents the intra- and intermolecular H bonds in hemicellulose or cellulose.[18] Meanwhile, the vibration at 3170 cm^{-1} changes after 3370 cm^{-1}, which also represents the NH_3^+ group.[30] Therefore, this suggests that, in the early reaction at low temperatures, H in holocellulose first transitions to R−NH_2 in protein and then forms the NH_3^+ group. In addition, the vibration at 1595 cm^{-1} changes before 1430 cm^{-1}, which represents an aromatic ring bend in the lignin.[18,22] As shown in Figure 4, the intensity of the aromatic ring bend dramatically increases at 250−450 °C, which may be due to the degradation of holocellulose, and subsequently, this group is rapidly removed at 450−650 °C, which may be due to the degradation of lignin.[31] The above description indicates that the high N content has a dramatic effect on the formation of char.

Figure 5 shows the Raman peak areas and band ratios as functions of the temperature for the chars. The obtained Raman spectra begin at 450 °C, which may be because the fused ring structure rarely occurs at low temperatures, and then no inelastic scattering of incident photons was induced.[33,34] The total Raman intensity decreases with the temperature increase, which may be caused by the loss of heterogeneous atoms (O−, N−, and S−).[33] The D band intensity increases, while the G band intensity slightly decreases over the investigated temperature range; hence, the I_G/I_D ratio shows a decrease. This indicates that the concentration of aromatic rings having 6 or more fused benzene rings increases, and this structure may be derived from both the dehydrogenation of hydroaromatics and the growth of aromatic rings.[15] The amorphous structures (relatively small aromatic ring systems possessing 3−5 fused benzene rings), represented by G_R, V_L, and V_R, increase slightly at 450−550 °C and subsequently continue to decrease. The band area ratio between the $G_R + V_L + V_R$ band and the D band continues to decrease, suggesting that these relatively small aromatic ring systems are converted to large aromatic ring systems with the increase in the temperature.[15,33] The high N content in chars is also reflected by the Raman spectra. The combined $S_l + S + S_r + R$ band generally decreases with a low N content of chars because the branched structures represented by this band may be removed by an increase in the temperature.[33] However, a contrast is observed for tobacco waste chars in that the intensity of the combined $S_l + S + S_r + R$ band increases at 650−850 °C. Furthermore, it is notable that the degree of increase of the combined $S_l + S + S_r + R$ band is larger than that of the D band; therefore, the band area ratio between the combined $S_l + S + S_r + R$ band and the D band also shows a significant increase at 650−850 °C. It is suspected that N can influence the formation of the aromatic structure in char. During formation of the fusing aromatic structure, N would move to the edge of these fusing aromatic structures and then form a heterocyclic structure. With the enlarged size of the aromatic cluster containing N, the N atom may replace C and form an embedded defect in the carbon structure.

In summary, through the combined results of FTIR and FT−Raman, the formation mechanism of tobacco waste char during pyrolysis is followed. The char formation process can be divided into three stages. During the first stage, from 250 to 450 °C, the raw biomass converts to a network-like structure, whose basic node is the fusing aromatic with 1−2 aromatic rings with connection of functional groups containing methyl, methylene, and oxygen. The second stage occurs when the

DOI: 10.1021/acs.energyfuels.5b02255
Energy Fuels 2016, 30, 1579−1588

Table 3. Pore Structure and Adsorption Property of Chars for Different Feedstocks

temperature (°C)	250	350	450	550[a]	650	750	850[a]	950
Pore Characteristic								
S_{BET} (m^2/g)	1.14	1.38	3.33	2.87	5.12	65.63	266.03	361.07
Adsorption Capacity (mg/g)								
water	214.7	564.6	462.7	437.6	451.0	457.7	287.4	199.6
phenol	0.45	1.02	1.89	3.42	3.76	4.68	6.11	9.28

[a]The data were repeated, and the errors were below 10%.

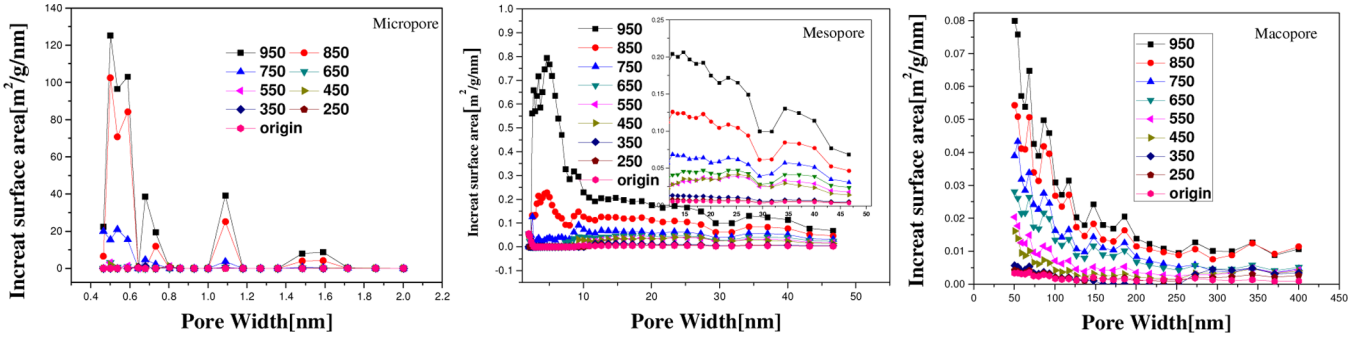

Figure 6. Pore size distribution derived from the N_2 adsorption by DFT. This analysis was not repeated because the analyzing time was very long (up to 72 h for each trial) and almost half of received chars was used.

temperature increases to 550 °C, during which the cleavage reaction of the functional groups containing methyl, methylene, and oxygen provides a greater chance of contact with the fusing aromatic, which leads to an increase from 1−2 to 3−5 rings of fused aromatics. With the continued increase in the temperature, from 550 to 950 °C, condensation, including the dehydrogenation and cleavage of ether bonds, promotes enlargement of the fusing aromatic structure up to ≥6 rings.

The evolution of the pore structure for chars at various temperatures is shown in Table 3 and Figure 6. The surface area (S_{BET}) of raw tobacco waste is 3.21 m^2/g, while the chars at 250 and 350 °C have S_{BET} < 2 m^2/g. The amounts of macro-, meso-, and micropores for these two chars are lower than those of the raw sample. This suggests that, during the initial degradation of tobacco waste, the original organic structure is damaged and the generated volatiles may block the original pores. At 450−650 °C, the chars show an increase in S_{BET}, from about 2 to 6 m^2/g; however, the increase in the surface area cannot capture the loss of volatiles, which has a significant potential to form more pores. It is observed that, in this temperature range, the increased number of pores is mainly distributed as macropores (50−100 nm) and mesopores (10−30 nm) compared to chars (<450 °C). The particle size distribution results indicate that this may be due to the escaped volatiles, which would be similar to peeling an onion. The notable pore formation begins at 650−750 °C. Char at 750 °C has 13 times the S_{BET} of char at 650 °C, and the micropores, particularly the 0.5−0.6 nm pores, show a dramatic increase in the number. Meanwhile, the number of meso- and macropores for this char also shows a notable increase. At this temperature, the particle size of char ceases to decrease; hence, it can be speculated that these pores may form as a result of the condensation and structure reforming reaction of char.[15] The pore formation process continues until 950 °C, and the pore blockage phenomenon[15] is not observed, although the ash content is extremely high. The increased number of pores at 850 and 950 °C shows a broad distribution of macro- and mesopores, while the micropore centers are 0.5, 1.1, and 1.5 nm. It is notable that the power spectral density (PSD) curve does not change and only the corresponding value increases, suggesting that the ash in chars may affect the pore formation and condensation and enlargement of the aromatic ring system may occur in the space limited by the ash structure.

The adsorption capacity of chars at various temperatures is also obtained. As Table 3 shows, the water adsorption is about 214.7 mg/g for the char at 250 °C, although the amount of pores is rather low. Furthermore, it is inconceivable that the char at 350 °C, which has a low number of pores, has the largest water adsorption value, up to 564.6 mg/g. When the temperature and number of pores increase, the water adsorption slightly decreases and a significant decrease of water adsorption is observed at 750−950 °C. The combined FTIR results indicate that the water adsorption capacity may be affected by the chemical functional groups, especially the basic N-containing groups. Meanwhile, in contrast with water adsorption, the phenol adsorption has a strong correlation with the amount of pores. The phenol adsorption of char increases with the temperature increase because more pores are formed.

3.3. Distribution and Transformation of Nitrogen in Products. The distribution of N in the char, gas, and liquid products during tobacco waste pyrolysis is shown in Figure 7. Cracking of N-containing compounds can be divided into three stages as the temperature is increased. First, when the temperature is <550 °C, N in the solid char decreases largely, while that in the liquid increases accordingly; however, no obvious change is present for the gas. This indicates that N quickly evolves from solid tobacco wastes but mainly condenses with liquid oil and little escapes as gas species. In combination with the FTIR structure of solid char, it can be observed that the amount of N residue in chars dramatically decreases with the increasing temperature. However, the lost N from chars is present in the liquid oil or gas at different stages. Below 550 °C, escaped N is dominant in the oil, while N in gas is rare. Between 550 and 650 °C, N in gas shows a significant increase from 5 to 28 wt %, while N in oil decreases to about 13 wt %

DOI: 10.1021/acs.energyfuels.5b02255
Energy Fuels 2016, 30, 1579−1588

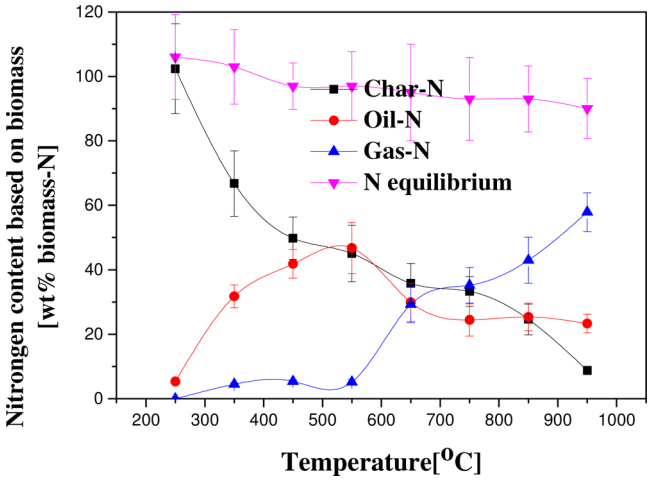

Figure 7. Distribution of the nitrogen content in the gaseous, liquid, and char products.

and that of char is about 7 wt %. This means that half of N in gas at 550−650 °C may be from the secondary decomposition of volatile N-containing compounds. When the temperature continuously increases from 750 to 950 °C, lost N from char may be converted directly into gas, while N in oil remains constant. The unbalanced N equilibrium may be caused by the undetected heavy weight composition in the liquid product, which generally condenses on the walls of the reactor and is difficult to collect.

The N chemicals detected in the gas product are NH_3 and HCN, which is consistent with other research on protein-enriched biomass.[35] As Figure 8 shows, the release of NH_3 and

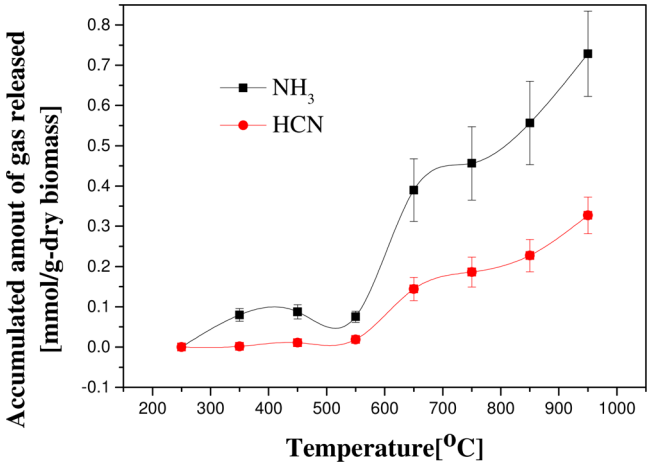

Figure 8. Released amount of gaseous nitrogen-containing compounds at different temperatures.

HCN may be divided into three stages. During the first stage, from 250 to 550 °C, NH_3 accumulates to about 0.1 mmol/g of dry biomass, while HCN is not detected. The combined FTIR results of chars indicate that NH_3 may be a result of the direct removal of NH_3^+ groups from char. During the second stage, from 550 to 750 °C, a significant quantity of NH_3 is released, with the concentration increasing from 0.1 to 0.45 mmol/g of dry biomass. Meanwhile, HCN is detected, and its concentration increases rapidly to 0.15 mmol/g of dry biomass. The formation of HCN may be from the cleavage of −CN bonds in chars and volatiles.[35] On the basis of the N distribution results, the dramatic release of NH_3 and HCN during this stage may be from the decomposition of unstable protein-derived volatiles.[20,35] In the final stage, NH_3 and HCN show a second increase to 0.72 and 0.3 mmol/g of dry biomass, respectively. At such a high temperature, the volatile-enriched protein fragment will break into low-weight molecules and the H_2-enriched atmosphere may lead to the formation of NH_3 and HCN.[36,37]

Table 4 shows the distribution of N-containing compounds in liquid oil at various temperatures. The result indicates that heterocyclic chemicals containing one N atom are the major N-containing compounds. There are two types of pyridines, those containing single pyridine rings and those containing double pyridine rings. At 550−650 °C, the pyridine content, particularly the single pyridine rings, reaches the peak value, while at higher temperatures, the single pyridine rings decrease. This may be due to the reaction between pyridine and chars; hence, the double-ringed pyridines, such as quinolone, increase at high temperatures. Pyrroles increase with the temperature increase, which suggests that the formation of pyrroles may be from the secondary reaction of N species with the volatiles or char. The maximum content of piperidines occurs at 750 °C, and the decrease of piperidines at temperatures >750 °C may be due to self-decomposition.

FTIR and FT−Raman are difficult to use to distinguish the detailed structural information on N-containing groups; hence, XPS analysis of several chars at 350, 550, 750, and 950 °C was carried out, and the results are shown in Figure 3S of the Supporting Information and Table 5. Three types of surface N-containing structures are distinguished, including pyridinic N (at 398.2 eV), pyrrolic/pyridine N (at 399.8 eV), and quaternary N (at 400.9 eV).[38,39] At 350 °C, pyrrolic/pyridine N is dominant at 76.34%, which may be the direct product of protein decomposition. With an increase in the temperature, the relative pyrrolic/pyridine N content decreases, pyridinic N and quaternary N increase, and the quaternary N, in particular, becomes the dominant structure at 750 and 950 °C. This suggests that C−N in pyrrolic/pyridine N may easily break and further condensation forms the pyridinic N; meanwhile, the close broken pyrrolic ring may connect to form quaternary N during the char or carbon formation reaction.[38]

4. CONCLUSION

The optimum temperatures for achieving high quantities of char, oil, and gas are 350, 550, and 750 °C, respectively. However, 650 °C is recommended as the optimum operating temperature for biomass pyrolytic polygeneration of tobacco waste when the three products are balanced. The best low calorific values of gas and char are 13 MJ/m^3 at 750 °C and 15 MJ/kg at 450 °C, respectively. N compounds were the major component of the organic parts of the liquid oil, up to 45%. The char formation process can be divided into three stages, including the degradation stage (250−450 °C), the reforming stage (450−650 °C) and the condensation stage (>650 °C). N-containing volatiles escape from chars with the temperature increase and are primarily found in liquid oil below 550 °C and gas above 650 °C. In gas, NH_3 and HCN are the major forms of N and are released above 650 °C. The major forms of N in liquid oil are pyridines, pyrroles, and piperidines, and the three types of N-containing structures formed in chars are pyridinic N, pyrrolic/pyridine N, and quaternary N. Pyridinic N is dominant at low temperatures; however, quaternary N becomes dominant at high temperatures.

DOI: 10.1021/acs.energyfuels.5b02255
Energy Fuels 2016, 30, 1579−1588

Table 4. Distribution of Nitrogen-Containing Composition in Liquid Oil from Variant Temperatures (Area % in GC−MS)

compound	temperature (°C)							
	250	350	450	550[a]	650	750	850[a]	950
pyridines	2.22	9.65	15.68	22.08	19.23	15.53	13.41	13.98
pyridine	0.00	1.67	2.55	2.21	2.13	2.28	2.65	2.22
pyridine, 3-methyl-	0.00	0.00	1.82	4.10	2.68	0.99	0.00	0.00
pyridine, 2-methyl-	0.81	0.64	0.70	1.54	0.94	0.90	0.00	0.00
quinoline	0.00	0.00	0.60	1.48	2.35	3.17	7.07	8.80
pyridine, 3-(3,4-dihydro-2*H*-pyrrol-5-yl)-	0.94	0.91	0.91	3.48	4.93	2.34	0.34	0.00
pyridine, 3-(1-methyl-2-pyrrolidinyl)-, (*S*)-	0.47	6.43	9.10	9.27	6.20	5.85	3.35	2.96
pyrroles	0	3.1	5.49	5.49	5.77	5.18	9.82	16.02
pyrrole	0.00	1.73	2.16	1.77	2.61	1.89	3.03	1.97
indole	0.00	0.75	0.55	0.62	1.10	2.11	6.79	14.05
4*H*-1,2,4-triazol-3-amine, 4-propyl-	0.00	0.62	2.78	3.10	2.06	1.18	0.00	0.00
piperidines	0.59	0.56	3.02	7.32	9.94	18.13	5.64	2.13
piperidine, 1-ethyl-	0.59	0.56	1.72	2.89	2.38	2.35	0.00	0.00
2,2,6,6-tetramethyl-4-piperidone	0.00	0.00	1.30	4.43	7.56	15.78	5.64	2.13
others	4.86	7.34	5.56	9.32	7.77	1.70	0.00	0.00
4,6-dihydroxy-2-methylpyrimidine	3.25	4.28	2.16	2.26	1.19	1.17	0.00	0.00
acetone cyanohydrin	1.61	3.06	3.40	7.06	6.58	0.53	0.00	0.00

[a]The data were repeated, and the errors were below 20%.

Table 5. Surface Nitrogen-Containing Structure by XPS Analysis

temperature (°C)	N 1s (area %)		
	N-1 (pyridinic N) 398.2 eV	N-2 (pyrrolic/pyridone N) 399.8 eV	N-3 (quaternary N) 400.9 eV
350		76.34	23.66
550[a]		46.99	53.01
750	26.44	11.79	61.77
950	28.42	9.27	62.31

[a]The data were repeated, and the errors were below 20%.

■ ASSOCIATED CONTENT

Supporting Information

The Supporting Information is available free of charge on the ACS Publications website at DOI: 10.1021/acs.energyfuels.5b02255.

2D-PCIS spectra in the range of wavenumbers of 3750−2700 and 1800−900 cm^{-1} analysis windows for chars (Figure 1S), typical example of curve fitting of a Raman spectrum of char obtained at 650 °C (Figure 2S), typical example of curve fitting of a XPS spectrum of char obtained at 550 °C (Figure 3S), and summary of Raman peak/band assignment representing the typical structures (Table 1S) (PDF)

■ AUTHOR INFORMATION

Corresponding Author

*Telephone: +086-027-87542417-8211. Fax: +086-027-87545526. E-mail: chenyingquan@hust.edu.cn.

Notes

The authors declare no competing financial interest.

■ ACKNOWLEDGMENTS

The authors express their great appreciation for the financial support from the National Natural Science Foundation of China (51406061), the Special Fund for Agro-scientific Research in the Public Interest (201303095), and the Key Projects of National Fundamental Research Planning (2013CB228102). The study also benefits from the technical support from the Analytical and Testing Center in Huazhong University of Science and Technology (http://atc.hust.edu.cn)

■ REFERENCES

(1) Briški, F.; Kopčić, N.; Ćosić, I.; Kučić, D.; Vuković, M. Biodegradation of tobacco waste by composting: Genetic identification of nicotine-degrading bacteria and kinetic analysis of transformations in leachate. *Chem. Pap.* **2012**, *66* (12), 1103−1110.

(2) Mumba, P. P.; Phiri, R. Environmental impact assessment of tobacco waste disposal. *Int. J. Environ. Res.* **2008**, *2* (3), 225−230.

(3) Wu, W. X.; Mei, Y. F.; Zhang, L.; Liu, R. H.; Cai, J. M. Kinetics and reaction chemistry of pyrolysis and combustion of tobacco waste. *Fuel* **2015**, *156*, 71−80.

(4) Fu, C.-q.; Tong, Y.-x.; Wang, F.-q.; Ren, T.-b.; Song, A.-d. Resources distribution and the utilization way of tobacco stem in China. *J. Cellul. Sci. Technol.* **2015**, *23* (2), 74−79 (in Chinese with an English abstract).

(5) Rincon, J.; De Lucas, A.; Garcia, M. A.; Garcia, A.; Alvarez, A.; Carnicer, A. Preliminary study on the supercritical carbon dioxide extraction of nicotine from tobacco wastes. *Sep. Sci. Technol.* **1998**, *33* (3), 411−423.

(6) Wang, S. N.; Xu, P.; Tang, H. Z.; Meng, J.; Liu, X. L.; Ma, C. Q. "Green" route to 6-hydroxy-3-succinoyl-pyridine from (S)-nicotine of tobacco waste by whole cells of a Pseudomonas sp. *Environ. Sci. Technol.* **2005**, *39* (17), 6877−6880.

(7) Akpinar, O.; Erdogan, K.; Bostanci, S. Enzymatic production of Xylooligosaccharide from selected agricultural wastes. *Food Bioprod. Process.* **2009**, *87* (C2), 145−151.

(8) Yang, Z. X.; Zhang, S. H.; Liu, L.; Li, X. P.; Chen, H. P.; Yang, H. P.; Wang, X. H. Combustion behaviours of tobacco stem in a thermogravimetric analyser and a pilot-scale fluidized bed reactor. *Bioresour. Technol.* **2012**, *110*, 595−602.

(9) Zhang, K.; Yu, B. T.; Chang, J.; Wu, G. Y.; Wang, T. D.; Wen, D. S. Hydrodynamics of a fluidized bed co-combustor for tobacco waste and coal. *Bioresour. Technol.* **2012**, *119*, 339−348.

(10) Zhang, K. H.; Zhang, K.; Cao, Y.; Pan, W. P. Co-combustion characteristics and blending optimization of tobacco stem and high-sulfur bituminous coal based on thermogravimetric and mass spectrometry analyses. *Bioresour. Technol.* **2013**, *131*, 325−332.

(11) Cardoso, C. R.; Miranda, M. R.; Santos, K. G.; Ataide, C. H. Determination of kinetic parameters and analytical pyrolysis of

DOI: 10.1021/acs.energyfuels.5b02255
Energy Fuels 2016, 30, 1579−1588

tobacco waste and sorghum bagasse. *J. Anal. Appl. Pyrolysis* **2011**, *92* (2), 392−400.
(12) Strezov, V.; Popovic, E.; Filkoski, R. V.; Shah, P.; Evans, T. Assessment of the Thermal Processing Behavior of Tobacco Waste. *Energy Fuels* **2012**, *26* (9), 5930−5935.
(13) Cardoso, C. R.; Ataide, C. H. Micropyrolysis of Tobacco Powder at 500 degrees C: Influence of $ZnCl_2$ and $MgCl_2$ Contents on the Generation of Products. *Chem. Eng. Commun.* **2015**, *202* (4), 484−492.
(14) Cardoso, C. R.; Ataide, C. H. Analytical pyrolysis of tobacco residue: Effect of temperature and inorganic additives. *J. Anal. Appl. Pyrolysis* **2013**, *99*, 49−57.
(15) Chen, Y. Q.; Yang, H. P.; Wang, X. H.; Zhang, S. H.; Chen, H. P. Biomass-based pyrolytic polygeneration system on cotton stalk pyrolysis: Influence of temperature. *Bioresour. Technol.* **2012**, *107*, 411−418.
(16) Chen, Y.; Yang, H.; Yang, Q.; Hao, H.; Zhu, B.; Chen, H. Torrefaction of agriculture straws and its application on biomass pyrolysis poly-generation. *Bioresour. Technol.* **2014**, *156*, 70−77.
(17) Yang, H.; Liu, B.; Chen, Y.; Chen, W.; Yang, Q.; Chen, H. Application of biomass pyrolytic polygeneration technology based on retort reactors. *Bioresour. Technol.* **2016**, *200*, 64−71.
(18) Chen, Y. Q.; Liu, B.; Yang, H. P.; Yang, Q.; Chen, H. P. Evolution of functional groups and pore structure during cotton and corn stalks torrefaction and its correlation with hydrophobicity. *Fuel* **2014**, *137*, 41−49.
(19) Li, X. J.; Hayashi, J.; Li, C. Z. FT-Raman spectroscopic study of the evolution of char structure during the pyrolysis of a Victorian brown coal. *Fuel* **2006**, *85* (12−13), 1700−1707.
(20) Mullen, C. A.; Boateng, A. A. Production and Analysis of Fast Pyrolysis Oils from Proteinaceous Biomass. *BioEnergy Res.* **2011**, *4* (4), 303−311.
(21) Yang, H. P.; Yan, R.; Chen, H. P.; Zheng, C. G.; Lee, D. H.; Liang, D. T. In-depth investigation of biomass pyrolysis based on three major components: Hemicellulose, cellulose and lignin. *Energy Fuels* **2006**, *20* (1), 388−393.
(22) Xin, S. Z.; Yang, H. P.; Chen, Y. Q.; Wang, X. H.; Chen, H. P. Assessment of pyrolysis polygeneration of biomass based on major components: Product characterization and elucidation of degradation pathways. *Fuel* **2013**, *113*, 266−273.
(23) Mohan, D.; Pittman, C. U.; Steele, P. H. Pyrolysis of wood/biomass for bio-oil: A critical review. *Energy Fuels* **2006**, *20* (3), 848−889.
(24) Oasmaa, A.; Solantausta, Y.; Arpiainen, V.; Kuoppala, E.; Sipila, K. Fast Pyrolysis Bio-Oils from Wood and Agricultural Residues. *Energy Fuels* **2010**, *24*, 1380−1388.
(25) Fu, P.; Yi, W. M.; Bai, X. Y.; Li, Z. H.; Hu, S.; Xiang, J. Effect of temperature on gas composition and char structural features of pyrolyzed agricultural residues. *Bioresour. Technol.* **2011**, *102* (17), 8211−8219.
(26) Neves, D.; Thunman, H.; Matos, A.; Tarelho, L.; Gomez-Barea, A. Characterization and prediction of biomass pyrolysis products. *Prog. Energy Combust. Sci.* **2011**, *37* (5), 611−630.
(27) Lee, Y.; Eum, P. R. B.; Ryu, C.; Park, Y. K.; Jung, J. H.; Hyun, S. Characteristics of biochar produced from slow pyrolysis of Geodae-Uksae 1. *Bioresour. Technol.* **2013**, *130*, 345−350.
(28) Shi, X. H.; Wang, J. A comparative investigation into the formation behaviors of char, liquids and gases during pyrolysis of pinewood and lignocellulosic components. *Bioresour. Technol.* **2014**, *170*, 262−269.
(29) Biederman, L. A.; Harpole, W. S. Biochar and its effects on plant productivity and nutrient cycling: A meta-analysis. *GCB Bioenergy* **2013**, *5* (2), 202−214.
(30) Rozenberg, M.; Shoham, G.; Reva, I.; Fausto, R. A correlation between the proton stretching vibration red shift and the hydrogen bond length in polycrystalline amino acids and peptides. *Phys. Chem. Chem. Phys.* **2005**, *7* (11), 2376−2383.
(31) Yuan, T.; Tahmasebi, A.; Yu, J. L. Comparative study on pyrolysis of lignocellulosic and algal biomass using a thermogravimetric and a fixed-bed reactor. *Bioresour. Technol.* **2015**, *175*, 333−341.
(32) Chaiwong, K.; Kiatsiriroat, T.; Vorayos, N.; Thararax, C. Study of bio-oil and bio-char production from algae by slow pyrolysis. *Biomass Bioenergy* **2013**, *56*, 600−606.
(33) Keown, D. M.; Hayashi, J.-I.; Li, C.-Z. Drastic changes in biomass char structure and reactivity upon contact with steam. *Fuel* **2008**, *87* (7), 1127−1132.
(34) Yip, K.; Xu, M.; Li, C. Z.; Jiang, S. P.; Wu, H. Biochar as a Fuel: 3. *Energy Fuels* **2011**, *25*, 406−414.
(35) Ren, Q. Q.; Zhao, C. S.; Chen, X. P.; Duan, L. B.; Li, Y. J.; Ma, C. Y. NO_x and N_2O precursors (NH_3 and HCN) from biomass pyrolysis: Co-pyrolysis of amino acids and cellulose, hemicellulose and lignin. *Proc. Combust. Inst.* **2011**, *33*, 1715−1722.
(36) Ren, Q. Q.; Zhao, C. S. NO_x and N_2O Precursors from Biomass Pyrolysis: Nitrogen Transformation from Amino Acid. *Environ. Sci. Technol.* **2012**, *46* (7), 4236−4240.
(37) Ren, Q. Q.; Zhao, C. S. NO_x and N_2O Precursors from Biomass Pyrolysis: Role of Cellulose, Hemicellulose and Lignin. *Environ. Sci. Technol.* **2013**, *47* (15), 8955−8961.
(38) Darvell, L. I.; Brindley, C.; Baxter, X. C.; Jones, J. M.; Williams, A. Nitrogen in Biomass Char and Its Fate during Combustion: A Model Compound Approach. *Energy Fuels* **2012**, *26* (11), 6482−6491.
(39) Liu, P.; Liu, W. J.; Jiang, H.; Chen, J. J.; Li, W. W.; Yu, H. Q. Modification of bio-char derived from fast pyrolysis of biomass and its application in removal of tetracycline from aqueous solution. *Bioresour. Technol.* **2012**, *121*, 235−240.

DOI: 10.1021/acs.energyfuels.5b02255
Energy Fuels 2016, 30, 1579−1588